Physics and Chemistry of Minerals (2022) 49:41
https://doi.org/10.1007/s00269-022-01215-4

ORIGINAL PAPER

Magnetic and structure transition of $Mn_{3-x}Fe_xO_4$ solid solutions under high-pressure and high-temperature conditions

Takamitsu Yamanaka[1,2] · Naohisa Hirao[3] · Yuki Nakamoto[4] · Takashi Mikouchi[5] · Takanori Hattori[6] · Kazuki Komatsu[7] · Ho-kwang Mao[2]

Received: 9 February 2022 / Accepted: 31 August 2022 / Published online: 11 October 2022

Abstract

Magnetic and structure transitions of $Mn_{3-x}Fe_xO_4$ solid solutions under extreme conditions are clarified by neutron time-of-flight scattering diffraction and X-ray Mössbauer measurement. The ferrimagnetic-to-paramagnetic transition temperature (100 °C) of Mn_2FeO_4 spinel is different from the tetragonal-to-cubic structure transition temperature (180 °C). The structure transition temperature decreases with increasing pressure. The transition is not coupled with the magnetic transition. Synchrotron X-ray Mössbauer experiments have revealed the pressure effects on the distribution of Fe^{2+} and Fe^{3+} at the tetrahedral and octahedral sites in the spinel structure. Ferrimagnetic $MnFe_2O_4$ and Mn_2FeO_4 spinels show sextet spectral features with hyperfine structure elicited by internal magnetic fields. Cubic $MnFe_2O_4$ spinel and tetragonal Mn_2FeO_4 transform to high-pressure orthorhombic postspinel phase above pressures of 18.4 GPa and 14.0 GPa, respectively. The transition pressure decreases with increasing Mn content. The postspinel phase has a paramagnetic property. Mn_2O_{10} dimers of two octahedra are linked via common edge in three dimentional direction. The occupancy of Fe^{2+} in the tatrahedral site is decreased with increasig pressure, indicating more oredered structure. Consequently, the inverse parameter of the spinel structure is increased with increasing pressure. The magnetic structure refinements clarify the paramagnetic and ferrimagnetic structure of $MnFe_2O_4$ and Mn_2FeO_4 spinel as a function of pressure. The magnetic moment is ordered between A and B sites with the anti-parallel distribution along the b axis. The nuclear tetragonal structure (a_N, a_N, c_N) has the ferrimagnetic structure but the orthorhombic magnetic structure has the ferrimagnetic structure with the lattice constants (a_M, b_M, c_M). The magnetic moment is ordered between A and B sites with the anti-parallel distribution along the b_M axis.

Keywords Magnetic structure analysis by neutron diffraction · Pressure dependence of the site occupancy · X-ray Mössbauer measurement at high pressure · Magnetic and structure transition under compression · Charge transfer of spinel at high pressure

✉ Takamitsu Yamanaka
t.yamanaka@cap.ocn.ne.jp;
takamitsu.yamanaka@hpstar.ac.cn

1 Department Earth and Space Science, Graduate School of Science, Osaka University, 1-1 Machikaneyama, Toyonaka 560-0043, Japan

2 Center for High Pressure Science & Technology Advanced Research, 1690 Cailun Rd Pudong, Shanghai 201203, China

3 Research and Utilization Division, Japan Synchrotron Radiation Research Institute (JASRI), SPring-8, 1-1-1 Koto, Sayo-cho, Sayo-gun, Hyogo 679-5198, Japan

4 Center for Science and Technology under Extreme Conditions, Osaka University, 1-3 Machikaneyama, Toyonaka 560-8531, Japan

5 The University Museum, University of Tokyo, 7-3-1 Hongo Bunkyo, Tokyo 560-0043, Japan

6 Materials and Life Science Division, Japan Proton Accelerator Research Complex (J-PARC), 2-4 Shirakata, Tokaimura, Naka-gun, Ibaraki 319-1195, Japan

7 Geochemical Research Center, Graduate School of Science, University of Tokyo, 7-3-1 Hongo Bunkyo, Tokyo 560-0043, Japan

Introduction

Important information about plate tectonics and geomagnetic reversals has been derived from measurements of remnant magnetization of spinels in basalts. Spinels are also the most fundamental magnetic compounds in industrial applications. Their magnetic properties, charge transfer and electrical resistivity changing under high-pressure conditions are significant research issues of intensive studies. The iron bearing spinels are the most fundamental magnetic compounds in industrial applications (Fei et al. 1999; Lavina et al. 1994; Jackson et al. 2005; Lin et al. 2013).

Structure analyses of the solid solution between Fe_3O_4 and Mn_3O_4 were conducted using thermal neutron diffraction by Hasting et al. (1956); Murasik et al. (1964). They are composed of mixed-charge cations in the tetrahedral (A) and octahedral (B) sites in AB_2O_4 spinels. Iron-rich members of the $Mn_{3-x}Fe_xO_4$ spinels have a magnetic structure of two-dimensional triangular Yafet-Kittel spin configuration reported by Yafet et al. (1952); Boucher et al. (1971); Gutzmer et al. (1995). Disorder of the cations in two sites has a great influence on magnetic properties such as saturation magnetization, exchange couplings and ferrimagnetic ordering temperatures.

Magnetite undergoes a phase transition to a high-pressure (HP) form, called h-Fe_3O_4. The stability field and the crystal structure of the HP magnetite, first, show a $CaTi_2O_4$-type structure with space group *Bbmm* (*Cmcm*) above 25 GPa, and second, defined to be $CaMn_2O_4$-type structure (*Pbcm*). Several experiments have been devoted to magnetite under high-pressure conditions by X-ray powder diffraction (Haavik et al. 2000; Kuriki et al. 2002; Dubrobinsky et al. 2003; Rozenberg et al. 2007; Reichmann et al., 2004). The Verwey transition temperature of Fe_3O_4 decreases non-linearly with increasing pressure (Todo et al. 2001). A big change in resistivity at the Verwey transition temperature was observed at pressure below 6.5 GPa. The pressure dependence of electrical resistivity of magnetite was measured under 100 GPa (Muramatsu et al. 2016).

The Néel temperatures of $Fe_{3-x}Mn_xO_4$ solid solutions at ambient pressure are: Fe_3O_4 (858 K), $MnFe_2O_4$ (563 K) and Mn_2FeO_4 (413 K) Mn_3O_4 (41.8 K). $Mn_{3-x}Fe_xO_4$ spinel structure transforms to a high-pressure phase of orthorhombic $CaMn_2O_4$-type postspinel structure. The transition pressures of the $Mn_{3-x}Fe_xO_4$ solid solution at ambient temperature are: Fe_3O_4 at 21.8 GPa, $MnFe_2O_4$ at 18.4 GPa and Mn_3O_4 at 10 GPa (Fei et al. 1999; Ye et al. 2015; Yamanaka et al 2022; Paris et al. 1992). The present neutron diffraction and X-ray Mössbauer spectroscopy shed light on the magnetic and structure change under extreme conditions.

$Mn_{3-x}Fe_xO_4$ spinel solid solutions are composed of mixed charged cations of Mn^{2+}, Mn^{3+}, Fe^{2+} and Fe^{3+} in the A and B sites in the AB_2O_4 spinel structure. In the $Mn_{3-x}Fe_xO_4$ solid solution, the spinel phase changes from cubic-to-tetragonal structure with increasing Mn content at ambient pressure. (Van Hook et al., 1958;McMurdie et al. 1950; Wickham 1969, Yamanaka et al. 1973).

Numerous investigations have been conducted on the temperature dependence of the cation distribution in $Mn_{3-x}Fe_xO_4$ spinel solid solution. (Hasting 1956; Rieck et al. 1966). Their phase stabilities and structures under extreme conditions have been studied. (Xu et al. 2004; Kirby et al., 1996; Yamanaka et al. 2001). The Curie temperature of Mn_3O_4 of about – 250 °C was reported by Boucher et al. (1971); Ole´s, et al. (1976); Chardon et al. (1986).

Curie temperatures in these spinels increase with increasing Fe content: 140 °C in Mn_2FeO_4 (synthetic ferrite), 290 °C in $MnFe_2O_4$ (jacobsite) and 585 °C in Fe_3O_4 (magnetite) (Nakagiri et al. 1986; Willerd et al. 1999).

In the present experiment, magnetic and structure studies of $MnFe_2O_4$ and Mn_2FeO_4 were conducted using neutron time-of-flight scattering diffraction under high-pressure condition at PLANET J-PARC (Hattori et al. 2015). Our previous Raman spectroscopic studies and synchrotron X-ray powder diffraction studies of various postspinels have proposed orthorhombic phases of $CaFe_2O_4$-type (*Pmma*), $CaTi_2O_4$-type (*Cmcm*) and $CaMn_2O_4$-type (*Pbcm*) structures as high-pressure polymorphs of different spinels (Yamanaka et al. 2008). Transformations of the oxide spinels are summarized in Table 1. These phases further transform to a new phase by martensitic transformation to a maximal isotropic subgroup structure.

X-ray structure analysis of $Mn_{3-x}Fe_xO_4$ causes an ambiguity, because X-ray atomic scattering factors of Fe (26) and Mn (25) are extremely similar. Neutron diffraction, however, has an effective advantage for the precise diffraction studies of $Mn_{3-x}Fe_xO_4$, because of the big difference in the coherent scattering lengths of Mn (– 3.73 fm) and Fe (9.54 fm). X-ray powder diffraction study at high pressures up to 40 GPa has been also performed by synchrotron radiation at Photon Factory using symmetric diamond anvil pressure cell (DAC) in this experiment.

Mössbauer spectroscopy (MS) study is the effective method to investigate the iron elctronic properties at high pressure. MS allows distingushing between ferric and ferrous ions. High and low spin states of Fe and their relative abundance in substances are clarified. MS studies of high-pressure Fe_3O_4 (h-Fe_3O_4) at ambient temperature have been carried out by Pasternak et al. (1994). The cation distributions in spinels at ambient conditions were reported by Mössbauer experiments and NMR studies (Yasuoka et al. 1967; Singh et al. 1981). Hyperfine-structure spectra changes of ferrites were reported as a function of pressure (Kobayashi et al. (2006).

Table 1 Transformations of the oxide spinels are summarized in three types. of $CaTi_2O_4$, $CaFe_2O_4$ and $CaMn_2O_4$

Transition pressure of high-pressure polymers of post spinel					
Compound	postspinel	Press (GPa)	method		reference
Cubic spinel-to-postspinel					
$ZnFe_2O_4$	CaFe2O4	24.6GPa	DAC	Raman	Z. Wang et al (2003a, b)
$ZnFe_2O_4$	CaMn2O4 or CaTi2O4	24.4GPa	quenched	XRD	D. Levy et al. (2000)
CoFe2O4	CaFe2O4	32.5GPa	DAC	Raman	Z. Wang et al (2003a, b)
MgFe2O4	CaMn2O4	24.6GPa	DAC	XRD	D. Andrault and N.B. Casanova (2001)
Fe3O4	CaTi2O4	24GPa	DAC	XRD	Y. Fei et al (1999)
Fe3O4	CaMn2O4	21.8GPa	DAC	XRD	C.Haaviketal (2000)
Fe3O4	CaTi2O4	2***	DAC	XRD	A.Ricolleau and Y. Fei (2016)
MgCr2O4	CaFe2O4	14.2GPa	DAC	Raman	Z. Wang et al (2002)
Fe2TiO4	CaTi2O4	16GPa	DAC	XRD	Y. Wu et al (2012)
	CaMn2O4		quenched	Möessbauer	
FeCr2O4	CaTi2O4	12-16GPa 1300℃	quenched	XRD	T. Ishii et al (2014)
Fe2TiO4	CaTi2O4	15GPa	quenched	XRD	M. Akaogi (2019)
MnFe2O4	CaMn2O4	18GPa	DAC	XRD	L. Ye (2015)
MnFe204	CaMn2O4	18GPa	DAC	NRD	Present work
MgAl204	CaTi2O4	25GPa	quenched	XRD	M. Akaogi (1999)
Tetragonal spinel-to-postspinel					
Mn3O4	CaMn2O4	7.2GPa 673 K	quenched	XRD	J. Darul (2013)
Mn3O4	CaMn2O4	10GPa	DAC	XRD	E. Paris (1992)
Mn2FeO	CaMn2O4	13GPa	DAC	NRD	Present work
MgMn2O4	CaMn2O4	30GPa	DAC	XRD	L. Malavasi (2005)
CoFe2O4	CaFe2O4	32.5GPa	DAC	XRD	Z. Wang (2003a)

Postspinels transform from $CaMn_2O_4$ to the $CaTi_2O_4$ structure with increasing pressure. The latter phase further transforms to new phase with multisite transformation by maximal isotropic subgroup structure change (Yamanaka et al. 2008)

The pressure dependence of the site occupancy and their magnetic structures were determined. In the present study, neutron diffraction at high pressure and high temperature has been conducted. The precise cation distribution has been elucidated by use of the significant difference in coherent scattering lengths between Mn and Fe. Furthermore. Fe^{2+} and Fe^{3+} distributions have been clarified by synchrotron X-ray Mössbauer experiments at increasing pressure. We also investigated the electrical resistivity measurement with increasing pressure up to 40 GPa to elucidate the enhancement of electrical conductivity from semiconductor to metal in $Mn_{3-x}Fe_xO_4$ spinel and postspinel with increasing pressure (Yamanaka et al. 2022). The observed enhancement of electrical resistivity with increasing pressure is shown in Supplement file 1.

Experiment

Powder samples of $MnFe_2O_4$ and Mn_2FeO_4 were prepared by solid–solid reaction at ambient pressure. To prepare the samples used for X-ray Mössbauer experiment, isotope-enriched samples with 30% ^{57}Fe content were prepared. The sample preparation is detailed in the supplement file 2.

Neutron diffraction experiment was executed a**t** BL-11 J-PARC (Japan Proton Accelerator Research Complex, Japan Atomic Energy Agency) under high-pressure using spallation neutron time-of-flight (TOF) facility. We used a Paris–Edinburgh (PE) press (VX4) for the experiments at pressures up to 40 GPa at room temperature (Hattori et al. 2019), and also a large-volume six-axis multi-anvil press ATSUHIME at PLANET J-PARC (Sano-Furukawa et al. 2014) for the experiments at pressures to 10 GPa and high temperatures up to 2000 ˚C. Incident neutron wavelength is 0.3 Å–5.8 Å and beam size is 15 mm × 15 mm at maximum.

We performed Rietveld analyses of neutron diffraction data to refine the nuclear structure and magnetic structure. The analysis is conducted using the program GSAS (Larson et al. 1994; Toby 2001). The integrated intensity I_o is produced by combination of magnetic scattering factor $F_M(\boldsymbol{h})$ and nuclear scattering factor $F_N(\boldsymbol{h})$:

$$I_o = s(h)A(h)L(h)m(h)\left\{|F_N(h)|^2 + |F_M(h)|^2\right\}, \quad (1)$$

where s: scale factor, A: absorption, L: Lorentz factor and m: multiplicity.

The nuclear structure factor F_N(h) for neutron diffraction is expressed by

$$F_N(h_k) = Sg_j b_{cj} T_j \exp|2pi(hx_j + ky_j + lz_j)|, \quad (2)$$

where T_j is the temperature factor of j atom. γ indicates the γ-factor of the nuclear magneton.

($\gamma = 1.913$). b is the scattering length ($b_{\mathrm{Mn}} = -3.73$ fm, $b_{\mathrm{Fe}} = 9.54$ fm).

And magnetic scattering factor $F_M(\boldsymbol{h})$ is

$$F_M(h_k) = ge^2/2mc^2\sqrt{1 - <\cos^2 h> xf(h_k)}\, Sg_j b_{cj} T_j \exp|2pi(hx_j + ky_j + lz_j)|,$$

$$\gamma \square e^2/2m_e c^2 = 2.696(fm), \quad (3)$$

where μ is magnetic moment.

The detailed derivation of the neutron diffraction refinement is presented in the Supplement file 3.

Neutron diffraction experiments cannot provide precise information about the distribution of Fe^{2+} and Fe^{3+} between the A and B sites in the Mn–ferrite spinel and the M1 and M2 sites of the postspinel structure under high pressure. We measured the synchrotron X-ray Mössbauer spectra of the $Mn_xFe_{3-x}O_4$ solid solution at SPring-8 BL-10XU (Hirao et al. 2020) under high pressure using micro-beam with the wavelength of 14.4 keV and diamond anvil cell (DAC). A symmetric diamond anvil cell was used to generate high pressure. Ne gas was used as a pressure transmitting media. Rh gasket of 200 µm thick was preindented to 80 µm. High-pressure measurement was performed by ruby-fluorescence scale.

We used the program MossA (Prescher et al. 2012) for the analysis of our Mössbauer spectra and determined the cation distribution as a function of pressure. Deviations from Lorentzian profile shape may have to be fitted using Voigtian (a convolution of Gaussian and Lorentzian functions). The full width half maxim (FWHM) of spectrum is related to the positional disorder of cations.

The isomer shift is referred to the spectrum from zero velocity of the ^{57}Fe spectrum in Fe_2O_3. The peak positions of the spectra were detected within an error of less than ± 0.05 mm/sec. The internal magnetic fields of the hyperfine structure spectra were determined with the reference of 26.26 T (330 kOe) of the ^{57}Fe in Fe_2O_3 spectrum.

Result and discussion

Pressure effect on the cooperative Jahn–Teller distortion of Mn_2FeO_4 spinel phase

$Mn_{3-x}Fe_xO_4$ spinel structure transforms to high-pressure phase of orthorhombic $CaMn_2O_4$-type postspinel structure. Present neutron diffraction study reveals the phase diagram of $Mn_{3-x}Fe_xO_4$ under high pressure at ambient temperature, which is presented in Fig. 1. Structure transition from tetragonal to cubic of Mn_2FeO_4 spinel under pressure at 20 °C is shown as a function of normalized unit-cell volume. Mn_2FeO_4 and $MnFe_2O_4$ spinel transform to postspinel at different pressures at 14.0 GPa and 18.4 GPa, respectively.

Present neutron diffraction patterns of Mn_2FeO_4 at 2.2 GPa in the heating experiment disclose the tetragonal-to-cubic transition temperature at 180 °C. The cooling experiments show the back transformation from cubic structure to the tetragonal structure at 140 °C. The tetragonal-to-cubic transition is reversible and shows hysteresis, as shown in Fig. 2.

Mn^{3+} ($3d^4$) prefers octahedral configuration in the strong ligand field. In the $Mn_{3-x}Fe_xO_4$ solid solution, Mn-rich phases present lattice distortion due to the cooperative Jahn–Teller (JT) effects. At ambient pressure, Mn_3O_4 transforms from tetragonal ($I4_1/amd$ z = 4) to cubic (Fd_3m z = 8)

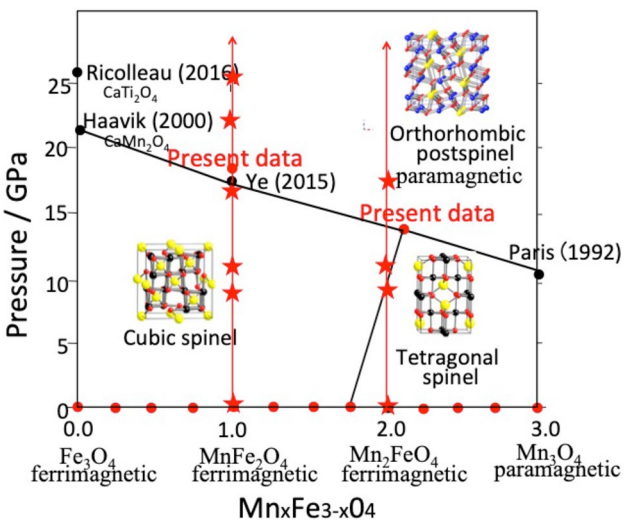

Fig. 1 Phase diagram of $Mn_{3-x}Fe_xO_4$ under high pressure at ambient temperature is presented by powder neutron diffraction study. Symbol of red stars indicate the X-ray Mössbauer experiment with increasing pressure in the present study at SPring-8. Plotted data with variable chemical compositions at ambient conditions are from Wickham et al. (1969) and Yamanaka ey al. (1973)

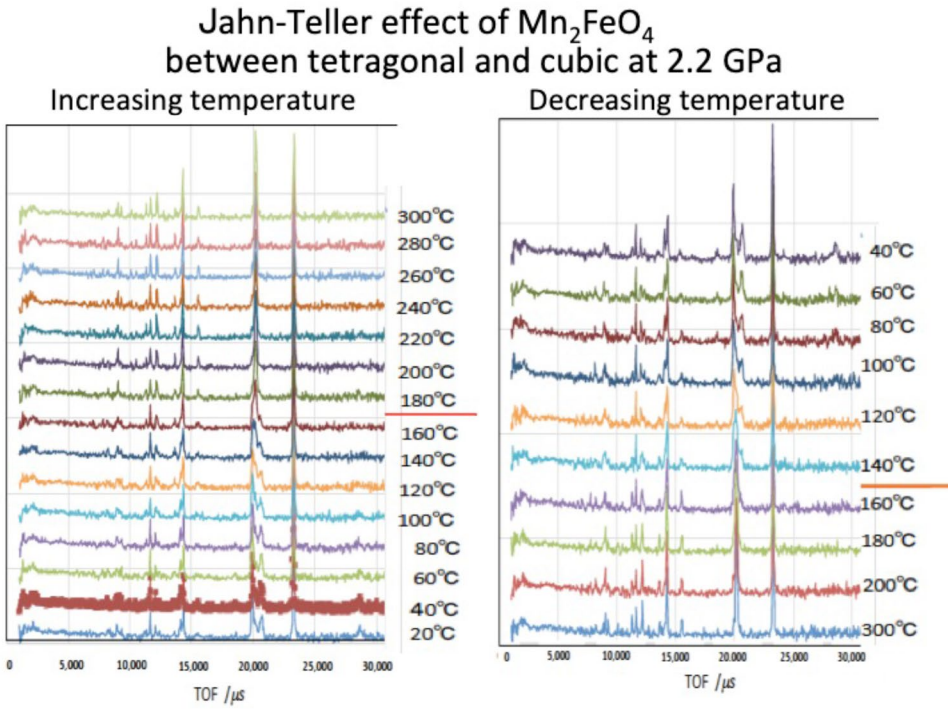

Fig. 2 Jahn–Teller effect degradation and appearance in Mn_2FeO_4 transition between tetragonal and cubic spinel spinels are shown. Neutron diffraction experiment of Mn_2FeO_4 at 2.2 GPa with increasing temperature confirms the tetragonal-to-cubic transition temperature at 180 °C. In the cooling experiments the cubic structure transforms back to the tetragonal structure at 140 °C. The tetragonal-to-cubic transition is reversible and shows a hysteresis of the transition

at 1170 °C (McMurdie et al. 1950) with vanishing JT effect. The phase has an elongated structure along the *c*-axis with $c/a > 1$.

The tetragonal-to-cubic transition temperature of Mn_2FeO_4 is 160 °C at 3 GPa and 180 ℃ at1GPa by the temperature dependence of *c/a*. These experiments prove the transition temperature decreases with increasing pressure. *P–T* boundary between the tetragonal and cubic phases has a negative slope. The distortion of the elongation along the *c*-axis disappears in the cubic Mn_2FeO_4. The lattice distortion may be reduced with increasing temperature and finally the lattice constant ratio becomes $c/a = 1$. resulting in the transformation to the cubic symmetry ($c = a$).

The two-phase mixtures with postspinel are found in the transition region (Fig. 3). The normalized unit-cell volumes of the three phases of cubic, tetragonal spinel and orthorhombic postspinel are shown in the figure. Both spinels have two-phase mixture regions with high-pressure postspinel phase.

The present transition case from tetragonal-to-cubic phase of Mn_2FeO_4 is extremely rare for the JT transition under compression. The following spinels: Fe_2TiO_4 (Yamanaka et al. 2013), $FeCr_2O_4$ (Kyono et al. 2011a, b), $ZnMn_2O_4$ (Choi et al. 2006), $CuMn_2O_4$ (Waskowska et al. 2001), $CuFe_2O_4$ (Kyono et al., 2015), $ZnGa_2O_4$ (Errandonea et al. 2009), $NiMn_2O_4$ (Åsbrink et al., 1988), transitions from cubic-to-tetragonal spinel show the with increasing pressure. Many of them have the tetragonal distortion with flattened octahedral distortion along the *c*-axis ($c/a < 1$). The octahedral site of the tetragonal phase of Mn_2FeO_4

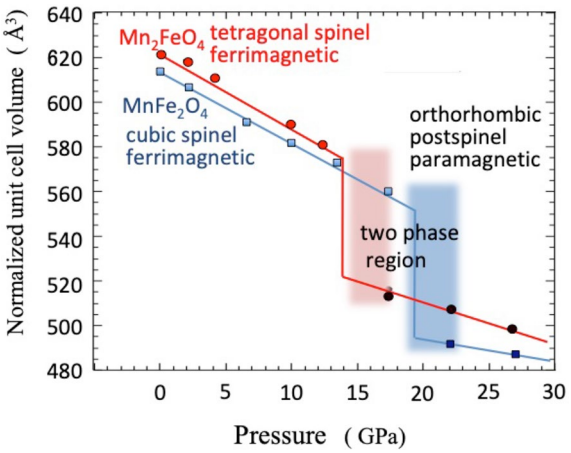

Fig. 3 Pressure dependence of the unit-cell volume of Mn_2FeO_4 and $MnFe2O_4$. Mn2FeO4 and $MnFe_2O_4$ transform to postspinel at pressures: 14.0 GPa and 18.4 GPa, respectively. Shadowed area indicates the two-phase mixture

is elongated along the *c*-axis and the lattice constant ratio $c/a > 1$ according to the crystal field stabilization energy (CFSE). Topological presentation is developed from the JT distortion. Pressure dependence of cooperative JT distortion in Mn_2FeO_4 is caused by localized orbital electronic states of Mn^{3+} under extreme conditions.

The result of the structure refinements of cubic $MnFe_2O_4$ and tetragonal Mn_2FeO_4 are presented in Supplement Table 1 and Supplement Table 2. The site occupancies are also presented in these tables. Their bond distances of A–O

and B–O together with AO_4 tetrahedral volume and BO_6 octahedral volume are presented in the tables.

The magnetic interaction is induced by supper exchange mechanism via oxygen. A–O and B–O bond distances and A–O–B bond angle are strongly related for the mechanism.

The compressions of the inter-nucleus distances A–A, A–B and B–B are strongly affected to the supper exchange. The B–B distance is much smaller than the other two A–A and A–B distances (Fig. 4). Then, the super-exchange between the B and the adjacent B cation is easier to gain extremely low resistivity. With compression, B–B shorter distance promotes a higher conduction. The B–B super-exchange model in the corner sharing octahedra is shown in Fig. 5. Super exchange for the electron hopping between Fe^{2+} and Fe^{3+} ion is more possible.

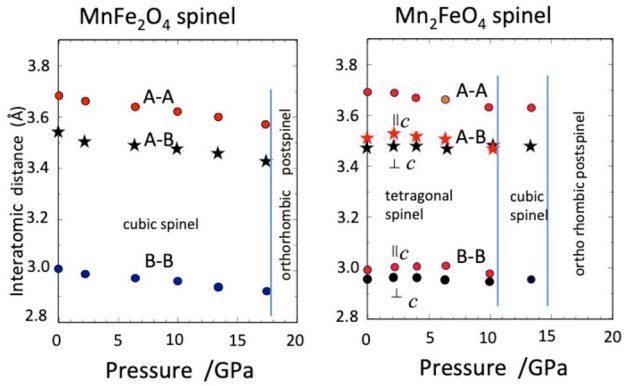

Fig. 4 Inter-cation distances A–A, B–B, and A–B in $MnFe_2O_4$ and Mn2FeO_4. The B–B distances in $MnFe_2O_4$ and Mn_2FeO_4 are much shorter than the A–A and A–B distances

Cation ordering

$MnFe_2O_4$ and Mn_2FeO_4 compounds are composed of the mixed-charge elements and their ionic radii are similar. According to the effective ionic radii (Shannon et al. 1969) and cation site preference (Duniz et al. 1957, 1960), positional change of these cations may be possible at high pressure. The distortions of the tetrahedral and octahedral sites make cation exchange possible by compression.

The cation exchange is common at high temperature and thermal atomic vibration is a strong mechanism for the cation positional change. Charge transfer in Fe^{2+}, Fe^{3+}, Mn^{2+} and Mn^{3+} is often observed in many experiments. Neutron diffraction studies show the change of the site occupancies at the A and B site and A–O and B–O distances at extreme high pressures. The bond distances at the A and B sites of Mn–O and Fe–O were evaluated through neutron diffraction study.

The site occupancies have a significant effect on electrical conductivity. The magnetic moments of the A and B sites in the $MnFe_2O_4$ and Mn_2FeO_4 spinel structures were also clearly observed. The inverse parameter i of the spinel structure in $(Mn^{2+}_{i}Fe^{3+}_{1-i})[Mn^{3+}_{1-i}Fe^{2+}_{1-i}Fe^{3+}_{2i}]O_4$ could be precisely defined for $MnFe_2O_4$. At high pressure, just before the transition pressures of the respective samples, they more closely adopt the normal spinel structure with $i=1$. The inverse parameter of $MnFe_2O_4$ is presented as a function of pressure in Fig. 6.

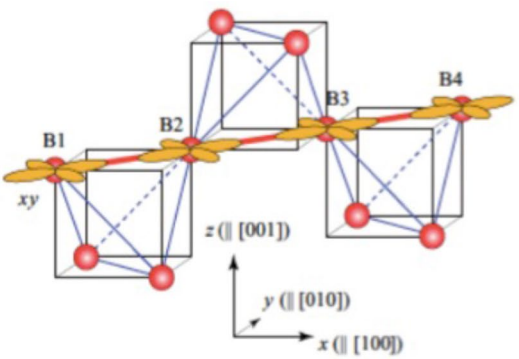

Fig. 5 Super exchange for the electron hopping between Fe^{2+} and Fe^{3+} ion is more possible in the B site than the A site. The super-exchange between B and the adjacent B cations is easier to gain extremely low resistivity. With compression, B–B shorter distance promotes a higher conduction. The B–B super-exchange model is shown in the corner sharing octahedra

Electron hopping

Fe_3O_4

$(Fe^{3+})[Fe^{2+}Fe^{3+}]O_4$

$MnFe_2O_4$

$(Mn^{2+}_{1-d}Fe^{3+}_{d})[Mn^{3+}_{d}Fe^{2+}_{d}Fe^{3+}_{2-2d}]O_4$

B - site

Mn_2FeO_4

$(Mn^{2+}_{1-d}Fe^{3+}_{d})[Mn^{3+}_{1+d}Fe^{2+}_{d}Fe^{3+}_{1-2d}]O_4$

B - site

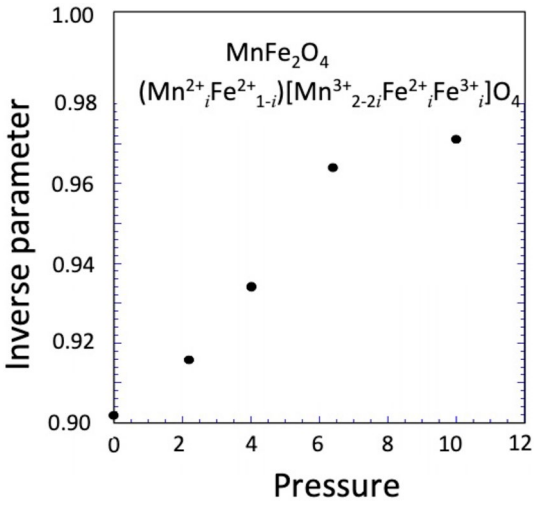

Fig. 6 Inverse parameter as a function of pressure of Mn_2FeO_4

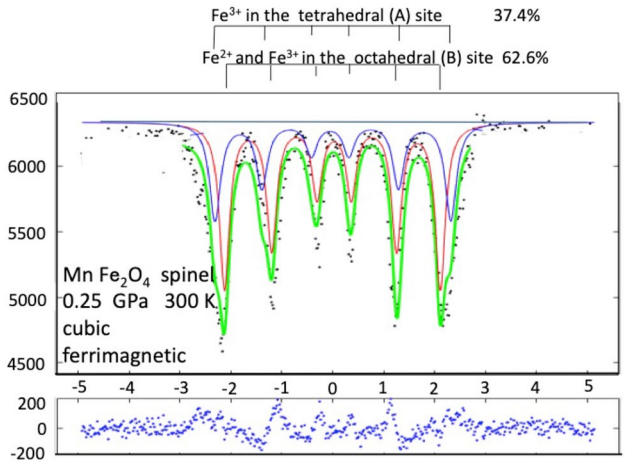

Fig. 7 Mössbauer spectrum of $MnFe_2O_4$ at 0.25GPa. Mössbauer spectrum of $MnFe_2O_4$ cubic spinel at 0.25 GPa and 300 K is shown. The spectra indicate two hyperfine structures of sextet patterns indicating ferrimagnetic moment of the A and B sites. The spectrum of the A site is assigned to Fe^{3+} in the tetrahedral site. The spectrum of the B site is assigned to mixture of Fe^{3+} and Fe^{2+} in the octahedral site. Intensity spectra ratio of the A and B site is presented

Mössbauer resonance experiment also shows Fe^{2+} and Fe^{3+} positional change in the A and B site at high pressure. Mössbauer spectra indicate two hyperfine structures of sextet patterns indicating ferrimagnetic moment of the A and B sites of $MnFe_2O_4$ cubic spinel at 0.25 GPa and 300 K in Fig. 7. The spectrum of the A site is assigned to Fe^{3+} in the tetrahedral site. The spectrum of the octahedral site (B) site is assigned to mixture of Fe^{3+} and Fe^{2+}. These Fe^{3+} and Fe^{2+} cations in the B site are not individually separated because of the electron hopping between these cations.

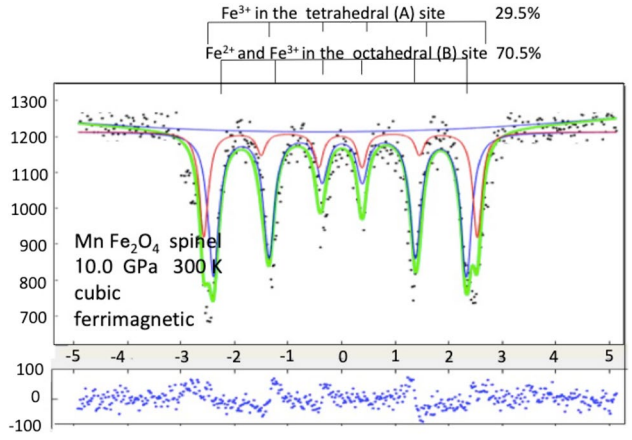

Fig. 8 Mössbauer spectrum of $MnFe_2O_4$ at 10.0 GPa and 300 K. Mössbauer spectrum of $MnFe_2O_4$ cubic spinel at 12.5 GPa and 300 K. The spectra show very similar hyperfine structures of sextet patterns to the spectra at 0.25 GPa shown in Fig. 5

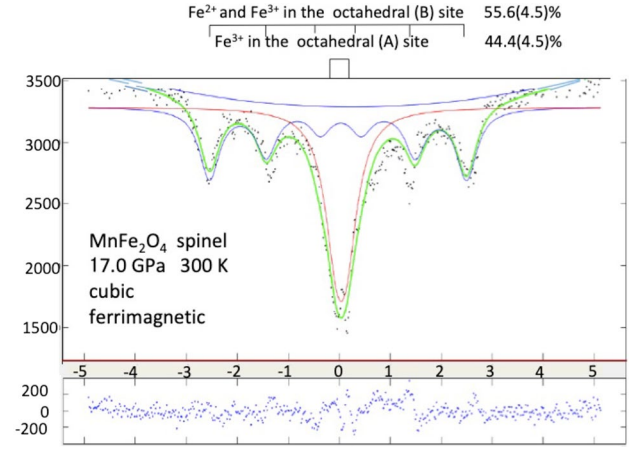

Fig. 9 Mössbauer spectrum of $MnFe_2O_4$ cubic ferrimagnetic phase at 17.0 GPa 300 K. One doublet indicates the Fe^{3+} spectrum at the tetrahedral site One sextet shows the Fe^{2+} and Fe^{3+} spectrum at the octahedral site are shown. The former spectrum proves neither hyperfine structure and nor internal magnetic field

Mössbauer spectra of $MnFe_2O_4$ cubic spinel at 10.0 GPa and 300 K are shown in Fig. 8 and they indicate two hyperfine structures of sextet patterns indicating ferrimagnetic moment of the A and B sites, which is a very similar spectra of the spectra in Fig. 7. Internal magnetic field observed from the both sextets at A and B sites are not changed between two pressures, 0.25 and 10.0 GPa.

Under further compression at 17.0 GPa 300 K shown in Fig. 9, Mössbauer spectrum of $MnFe_2O_4$ cubic ferrimagnetic phase shows one doublet indicates the Fe^{3+} spectrum at the A site and one sextet shows the Fe^{2+} and Fe^{3+} spectrum at the B site. The former spectrum proves neither hyperfine structure and nor internal magnetic field. The spectrum of

the hyperfine structure at the A site is not observed but the spectrum at the B site shows the internal magnetic field.

Neutron diffraction study of $MnFe_2O_4$ and Mn_2FeO_4 spinels indicates the ferrimagnetic cubic spinel structure at pressures up to 17.4 GPa and 14.0 GPa, respectively. Mössbauer spectra do not show any remarkable change up to 12.5 GPa. However, at 17.0 GPa the spectrum changes from sextet to doublet, proving neither hyperfine structure and nor internal magnetic field and magnetic moment of magnetic ions disappears, as shown in Fig. 9. Peak width of the sextet spectrum becomes broad at 17.0 GPa. The positional disorder of magnetic ions in the octahedral (B) site induces the peak broadening of the large FWHM in the spectrum.

Mössbauer spectra of the orthorhombic postspinel Mn_2FeO_4 at 18.0 GPa and 300 K have two doublets, as shown in Fig. 10. One indicates the sixfold octahedron indicating Fe^{3+} in the octahedral site (M2 site). Another doublet represents Fe^{2+} in the highly distorted eightfold large cation site (M1 site) with good reason of a large quadruple splitting. Two doublets of the Mössbauer spectra of postspinel indicate paramagnetic behavior. The result of Fe^{2+} and Fe^{3+} distributions in the ^{VIII}M1 and ^{VI}M2 sites is expressed by the following cation distribution: $^{VIII}[Mn^{2+}_{0.746},Fe^{2+}_{0.256}]^{VI}(Mn^{3+}_{0.628},Fe^{3+}_{0.372})_2O_4$. There is no sextet spectra in the postspinel phases of Mn_2FeO_4 and $MnFe_2O_4$ proving they are paramagnetic at high pressures.

In the Mössbauer spectra, the relative intensities of individual components possibly give a suggestion of the corresponding population. The intensities of the various peaks reflect the relative concentrations of cations. Observed site occupancies are estimated from the peak intensities of the Mössbauer spectra of $MnFe_2O_4$ and Mn_2FeO_4 at various

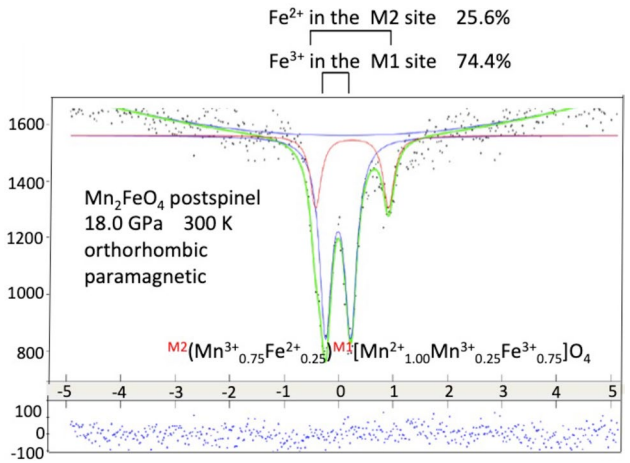

Fig. 10 Mössbauer spectrum of orthorhombic postspinel Mn_2FeO_4 spectra at 18.0 GPa. Two doublets are presented: Inner larger doublet indicates the sixfold octahedron, which is assigned to Fe^{3+} in the M2 site. Outer doublet represents Fe^{2+} in the highly distorted eightfold large cation site (M1 site) and postspinel is paramagnetic

pressures. The following data: (1) the isomer shift (δ), (2) the quadruple splitting (Δ) and (3) the magnetic hyperfine field (B_{hf}) are presented in Table 2. Peak intensity (Int) ratios of two or three spectra are also presented.

Two sextets of the spectra of $MnFe_2O_4$ cubic spinel at pressures from 1 atm to 12.5 GPa do not show a big difference in their peak intensities in Table 2 but show a slight increase in the intensity ratio with increasing pressure. The hypothetical structure proposed from the intensity ratio of two sextet spectra of the MS experiment gives the cation distribution, which is somewhat different from the result of the neutron diffraction structure analysis.

The distortion of Mn_2FeO_4 and $MnFe_2O_4$ spinels under compression are related to their elastic properties. The compression behavior of $Mn_{3-x}Fe_xO_4$ spinels can be described by third-order Birch–Murnaghan equation of state. The equation of state is given by

$$P(V) = \frac{3B_0}{2}\left[\left(\frac{V_0}{V}\right)^{7/3} - \left(\frac{V_0}{V}\right)^{5/3}\right] \left\{1 + \frac{3}{4}\left(B_0' - 4\right)\left[\left(\frac{V_0}{V}\right)^{2/3} - 1\right]\right\}, \quad (4)$$

where P is the pressure, V_0 is the reference volume, V is the deformed volume with respect to pressure,, B_0 is the bulk modulus, and B_0' is the derivative of the bulk modulus. The bulk modulus and its derivative are usually obtained from fits to experimental data and are defined as

$$B_o = -V(\partial P/\partial V)_{P=0} and B_o' = (\partial B/\partial P)_{P=0}. \quad (5)$$

The equations of state of $MnFe_2O_4$ and Mn_2FeO_4 show the difference in their transition pressures. Bulk modules of $Mn_{3-x}Fe_xO_4$ spinel solid solutions are presented in Table 3.

$MnFe_2O_4$ and Mn_2FeO_4 are characterized by cation disorder and are more compressible than the end-members of the solid solution. $MnFe_2O_4$ is less compressible than Mn_2FeO_4.

High-pressure polymorph postspinel phase

Magnetite undergoes a phase transition to a high-pressure (HP) form, called h-Fe_3O_4 above 25 GPa and defined to be postspinel of $CaMn_2O_4$ (*Pbcm*) structure. Postspinel is characterized by herringbone structure, shown in Fig. 11. The present X-ray Mössbauer spectra analyses and neutron diffraction experiments describe the cation distributions of Mn and Fe. The structure refinements of postspinel of Mn_2FeO_4 at pressures up to 26.8 GPa are presented in Supplement Table 3. (The refinement of the quenched sample is also presented in the table.) The ^{VIII}M1 site volume is much larger than the ^{VI}M2 site. The ^{VIII}M1 site of Mn_2FeO_4 and $MnFe_2O_4$ postspinel is mostly occupied by

Table 2 Mössbauer spectra analyses of $MnFe_2O_4$ (cubic spinel), Mn_2FeO_4 (tetragonal spinel) and postspinel ($CaMn_2O_4$ type) of Mn_2FeO_4

Mössbauer resonance spectra under high pressure							
$MnFe_2O_4$ spinel compound							
Pressure	structure	Site	ion	σ mm/s	Δmm/s	Int %	B_{HF}
0.0001 GPa	Tetra	^{IV}A	Fe^{3+}	0.028(0.032)	0.017(0.020)	34.3(0.5)	480(6)
		^{VI}B^{+}	Fe^{2+} + Fe^{3}	– 0.056(0.016)	0.035(0.056)	65.7(0.8)	456(12)
2.5 GPa cubic	Cubic	^{IV}A	Fe^{3+}	– 0.021(0.18)	0.054(0.037)	30.4(0.6)	479(10)
		^{VI}B	Fe^{2+} + Fe^{3+}	0.013(0.14)	0.034(0.027)	69.6(0.6)	444(7)
10.0GPa	Cubic	^{IV}A	Fe^{3+}	– 0.019(0.013)	0.005(0.025)	29.6(0.3)	513(10)
		^{VI}B	Fe^{2} + Fe^{3+}	– 0.008(0.008)	0.044(0.065)	70.9(0.3)	495(8)
12.5GPa	Cubic	^{IV}A	Fe^{3+}	0.018(0.009)	0.091(0.028)	29.1(0.8)	542(10)
		^{VI}B	Fe^{2+} + Fe^{3+}	– 0.017(0.008)	– 0.036(0.014)	70.9(0.8)	502(8)
17.0GPa	Cubic	^{IV}A	Fe^{3+}	0.036(0.058)	0.003(0.027)	44.4(4.5)	
		^{VI}B	Fe^{2+} + Fe^{3+}	– 0.008(0.015)	0.034(0.027)	55.6(4.5)	523 (10)
Mn_2FeO_4 spinel compound							
Pressure	Structure	Site	Ion	σ mm/s	Δmm/s	Int %	B_{HF} Oe
0.0001GPa	Tetra	^{IV}A	Fe^{3+}	0.072(0.032)	0.032(0.020)	12.3(1.5)	366(12)
		^{VI}B	Fe^{2+} + Fe^{3+}	0.056(0.016)	0.025(0.056)	87.7(2.8)	406(7)
10.0 GPa	Tetra	$^{I V}$A	Fe^{3+}	– 0.094(0.029)	0.668(0.024)	5.9(2.8)	
		^{VI}B	Fe^{2+}	– 0.034(0.016)	0.018(0.056)	7.5(2.8)	
		^{VI}B	Fe^{2+} + Fe^{3+}	– 0.034(0.016)	0.018(0.056)	86.6(2.8)	437(12)
Postspinel ($CaMn_2O_4$ type) of Mn_2FeO_4							
Pressure	Structure	Site	Ion	σ mm/s	Δmm/s	Int %	B_{HF} Oe
18.0 GPa	Ortho	^{VIII}M1	Fe^{2+}	– 0.253(0.014)	1.338(0.028)	25.6(3.2)	–
		^{VI}M2	Fe^{3+}	– 0.004(0.061)	0.461(0.011)	74.4(3.2)	–

The isomer shift (IS), quadruple splitting (QS), relative intensity (Int) and internal magnetic field (BIF) of each site of $MnFe_2O_4$ spinel are presented in the table spinel

σ isomer (chemical) shift, Δ quadruple splitting, *Int* intensity ratio of area ratio of two spectra. *BIF* hyperfine magnetic field

The number in parentheses is the error of the last decimal. (1kOe = 103/4π[kA/m)

Mn^{2+}, which increases with increasing pressure. The ^{VI}M2 site of $MnFe_2O_4$ is occupied by mainly Fe and only small amount of Mn. On the other hand, the ^{VI}M2 of Mn_2FeO_4 is half-occupied by Mn. The phase of Mn_2FeO_4 is composed of an almost ideal ordered structure of $^{VIII}[Mn^{2+}]^{VI}(Mn^{3+}{}_{0.5}Fe^{3+}{}_{0.5})_2O_4$. The atoms in the ^{VI}M2 site are located on the edge-sharing plane perpendicular to the *c*-axis, as shown in Fig. 11. Mn_2O_{10} dimers of two octahedra in the structures are linked via common edges.

Magnetic structure of Mn_2FeO_4 and $MnFe_2O_4$ spinel

Present magnetic structure analysis of Mn_2FeO_4 and $MnFe_2O_4$ as a function of pressure is executed using the neutron diffraction intensity I_o. Integrated intensity I_o is a combination of both magnetic scattering factor $|F_M(\boldsymbol{h})|^2$ and nuclear scattering factor $|F_N(\boldsymbol{h})|^2$ by Eq. (1). Present Rietveld refinement based on the ferrimagnetic structure discloses the tetrahedral and octahedral symmetry of the tetragonal-to-cubic transition with increasing pressure. The site symmetry 0.2 *m*. of the octahedral (B) site in the tetragonal symmetry of $I4_1/amd$ changes to the symmetry of._3*m* of the cubic symmetry of *Fd*_3*m*.

The diffraction peaks of 101 and 112 of tetragonal phase have a large contribution of magnetic scattering. The temperature evolution of the diffraction intensity of Mn2FeO4 at ambient pressure indicates that both peak intensities suddenly drop around 100 °C, which is displayed in Fig. 12. The magnetic transition temperature at 100 °C of ferrimagnetic-to-paramagnetic is different from the tetragonal-to-cubic structure transition temperature at 180 °C. The magnetic transition temperature is lower than that of the nuclear structure transition. The structure change is not coupled with magnetic transition.

Table 3 Bulk modulus of $Mn_{3-x}Fe_xO_4$ spinel solid solutions are presented

Bulk modulus of Fe_3O_4 – Mn_30_4 solid solution				
Samples	B_o (GPa)	B_o'	Ref. & Remark	
Fe_3O_4	172	4 (fixed)	Ricolleau and Fei (2016)	
	217	4 (fixed)	Haavik et al. (2000)	
$MnFe_2O_4$	155.8 (8)	4.9(1.1)	Present study (χ^2=0.009 R=0.99)	
	169(45)	2.87(40)	Ye et al. (2015)	
Mn_2FeO_4	104.2(34)	3.9(0.7)	Present study (χ^2=0.104 R=0.99)	
Mn_3O_4	132.6(1.3)	4 (fixed)	Darul et al. (2013)	
Bulk modulus of A and B site of MnFe2O4 and Mn2FeO4				
MnFe2O4 Cubic spinel				
Bulk and Site	B_o (GPa)	B_o'	Refinement	resolution
Bulk	155.8(8)	4.9(1.1)	χ^2=1.0002	R=0.9997
AO_4	154.94(8)	6.67(2.15)	χ^2=1.354	R=0.996
BO_6	184.9(14)	6.68(2.57)	χ^2=0.585	R=0.9996
Mn_2FeO_4 tetragonal spinel				
Unit cell and Site	B_o (GPa)	B_o'	Refinement	resolution
Bulk	103.2 (34)	2.974(0.7)	χ=0.336	R=0.9971
AO_4	142.9(21)	5.038(4.98)	χ^2=1.485	R=0.9941
BO_6	155.6(35)	3.266(6.71)	χ^2=1.629	R=0.9945

The values of *Bo* and *B'* are changed with the site occupancy of Mn and Fe at the A and B sites. The equations of state of $MnFe_2O_4$ and Mn_2FeO_4 show the difference in their transition pressure

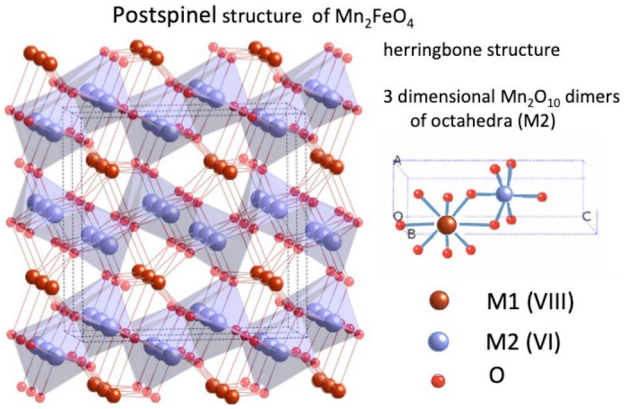

Fig. 11 Postspinel is constructed by herringbone structure of the M1 octahedra array. The dimer of octahedra is distributed in three-dimensional space. eightfold M2 cation has shared edges with M1 cation and chained in the direction of the *b* axis

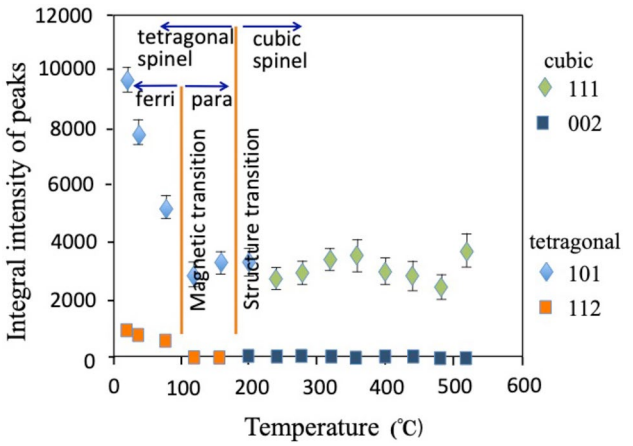

Fig. 12 Difference in the transition temperature between the magnetic (ferrimagnetic-to-paramagnetic) and structure (tetragonal-to-cubic) transition of Mn_2FeO_4. Magnetic transition temperature is 100 °C and structure transition temperature is 180 °C

The present magnetic refinement shown in Table 4 confirms the site occupancies at the A and B sites of Mn_2FeO_4 postspinel under elevating pressure. Magnetic moment distribution of the spinel and postspinel structure requires the effective magnetic susceptibility of cations. Effective Bohr magneton is used from extant published data defined by previous experiments: Mn^{2+} (5.92 μB), Mn^{3+} (4.90 μB), Fe2+ (4.90 μB) and Fe3+ (5.92 μB) (Neel 1948). Iron-rich members of the Mn3-xFexO4 spinels have the magnetic structure of two-dimensional Yafet-Kittel triangular spin configuration. The magnetic structure of a powder sample of $MnFe_2O_4$ was determined by thermal neutron diffraction (Levy 2015). Spin moments of the A and B sites of the

Table 4 Magnetic moment and site occupancy at the A and B sites of tetragonal Mn_2FeO_4 spinel

Lattice constant			site occupancy			magnetic moment			$\chi 2$	R(F^2)
Press(GPa)	a (Å)	c (Å)	Vol (Å^3)	Mn(tet)	Mn(oct)	A(tet)	B(oct)	total		
0.0001	5.9453	8.7844	10.98	0.902	0.548	− 2.002	4.655	2.653	2.173	0.222
2.2	5.9466	8.7498	309.41	0.916	0.542	− 1.186	3.314	2.128	2.957	0.167
4	5.9392	8.6494	305.1	0.934	0.533	− 0.077	2.043	1.966	3.866	0.178
6.4	5.9232	8.5094	301.39	0.964	0.524	− 1.556	3.166	1.61	3.099	0.139
10	5.9106	8.4167	294.69	0.962	0.519	− 2.003	3.381	1.378	6.239	0.211

Ferrimagnetic magnetic moments of individual A and B sites are shown. And the moment in the unit cell is presented in total. X^2 and $R(F^2)$ are accuracy parameters in the magnetic structure refinement

iron substitution on the magnetic property were clarified at temperatures 10 K and 295 K (Baron et al. 1998).

The influence of iron substitution on the magnetic properties is clarified in both ordered and disordered ferrimagnetic spinel-phases. Magnetic cations of Mn and Fe are located at the crystallographically special position in the tetragonal and cubic structure. Positional parameters of these cations are variable and magnetic moments are also variable parameters besides thermal variables. The reliability factor for the refinement is enhanced by the inclusion of magnetic moment effect. Nuclear structure analysis without consideration of magnetic moment effect was not converged properly.

Several possible magnetic space groups in nine subgroups of the tetragonal spinel structure of $I4_1/amd$ are examined for the observed intensities. The magnetic space group of $I4_1/am'd'$ is the most reliable subgroup of the space group symmetry of $I4_1/amd$. Rietveld refinement of Mn_2FeO_4 at 2.2 GPa 20 ℃ tetragonal $I4_1/amd$ with the paramagnetic structure model is $\chi^2 = 10.51$ and R(F2) = 0.211. We analyzed the diffraction intensities of the observed data in this study, because the quality of the data taken at high pressures in this study is not sufficient to discuss the detail of counted spins. The ferrimagnetic structure model based on the orthorhombic space group Pmma, (which is of an isomorphic subgroup of I41/amd) shows much better agreement of $\chi^2 = 2.157$ and $R(F^2) = 0.117$. The lattice constants (a_M, b_M, c_M) of Mn_2FeO_4 of the present orthorhombic ferrimagnetic structure are derived from the nuclear tetragonal structure (a_N, a_N, c_N). The b_M cell edge is twice larger than b_N of the paramagnetic lattice, because the magnetic moment is ordered between A and B sites with the anti-parallel distribution along the b_M axis. The Rietveld analysis is shown in Fig. 13. The distribution of the anti-parallel magnetic spins in A and B site are presented in the figure. Pressure dependence of site occupancy and magnetic moment of the ferrimagnetic Mn_2FeO_4 spinel are summarized in Table 4. The site occupancies of Mn at the tetrahedral and octahedral sites of Mn_2FeO_4 and $MnFe_2O_4$ spinels are shown with increasing pressure. The cation distribution becomes close to the ordered normal spinel structure. Ferrimagnetic spin moment

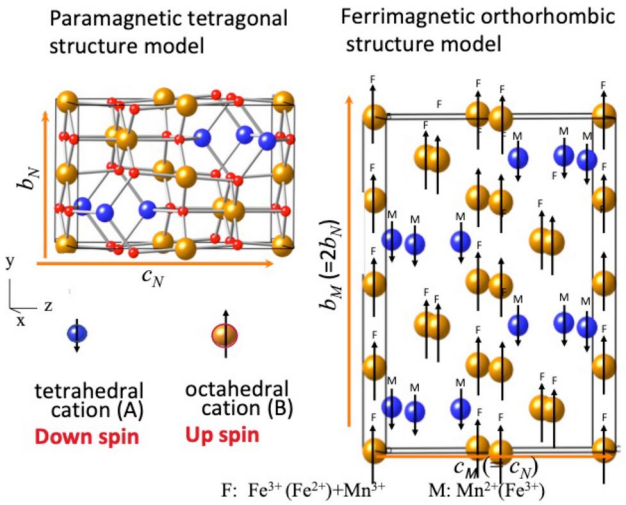

Fig. 13 Paramagnetic Mn_2FeO_4 tetragonal structure at 2.2 GPa is shown in the left figure. Right figure shows anti-parallel magnetic spin moments along the c_M axis of the ferrimagnetic Mn_2FeO_4 orthorhombic structure at 2.2 χ^2R(F^2) = 0. 117). Only cations are presented in the figure. They are similar positions in the paramagnetic tetragonal structure. Ferrimagnetic lattice has a_M, b_M, $c_{M.}$, and b_M is twice large b_N of the paramagnetic lattice

becomes smaller at higher pressure before the transformation to the high-pressure postspinel phase.

Pressure dependence of magnetic structure was suggested by X-ray Mössbauer experiment. Deviations from ian profile may be induced from variations of local environments or fluctuations of parameters.

Conclusion

Magnetic studies of minerals are reliable witnesses of paleomagnetism by high-resolution studies of these structures. The magnetic structures are built during the cooling of molten rock and reflect the earth's magnetic field at the time of their formation. This record provides information on the past behavior of Earth's magnetic field and geomagnetic reversal. The magnetic properties are reset by the interaction

of the magnetic spin inside the Earth's magnetic field. The geomagnetic reversal is an indicator of magnetic field change in plate tectonics. However, the pressure effect of the plate tectonics still remains to be seen in the magnetic study of minerals.

The present neutron diffraction and synchrotron X-ray Mössbauer spectroscopic study provide the comprehension of the magnetic and structure change under extreme conditions. Some of oxide spinels with transition elements have a ferrimagnetic property at ambient conditions. They transform to the postspinel structures under high-pressure condition. Cation distributions in $Mn_{3-x}Fe_xO_4$ solid solutions under extreme conditions are significant research subjects not only for geophysical understands such plate tectonics and geomagnetic reversals but also for the basic magnetic ferrite industrial materials. Magnetic and structure transition studies are possible by neutron time-of-flight scattering diffraction at PLANET J-PARC. Besides the neutron diffraction, X-ray Mössbauer experiment is a significant and complementary study to investigate the magnetic property of $Mn_{3-x}Fe_xO_4$ solid solutions from the hyperfine structure of Zeeman splitting. The present experiments disclosed the following new discoveries of magnetic properties:

(1) The lattice distortion is not coupled with magnetic transition. The magnetic transition temperature from ferrimagnetic-to-paramagnetic of spinels is lower than the structure transition temperature from tetragonal-to-cubic structure transition. The structure transition temperature decreases with increasing pressure.

(2) Pressure dependence of cooperative Jahn–Teller distortion in Mn_2FeO_4 is observed by the interaction between localized orbital electronic states of Mn^{3+} and the compression of the octahedral site. The transition temperature from tetragonal-to-cubic phase decreases with increasing pressure. The transition of Mn_2FeO_4 is an extremely rare case for the JT transition with increasing pressure. Generally many spinels show cubic-to-tetragonal transition at high pressure and the tetragonal distortion is of flattering octahedral distortion of $c/a < 1$, However, the tetragonal phase of Mn_2FeO_4 shows the transformation from tetragonal-to-cubic and the octahedral site is elongated along to the *c*-axis and the lattice constant ratio is $c/a > 1$.

(3) Inverse parameter change under compression.

X-ray Mössbauer measurement and nuetron diffraction study confirm that the occupancy of Fe^{2+} in the tatrahedral site is decreased with increasig pressure, indicating more oredered structure. The inverse parameter is increased with increasing pressure.

(4) The cubic $MnFe_2O_4$ spinel and tetragonal Mn_2FeO_4 transform to the high-pressure orthorhombic postspinel phase at pressure 18.4 GPa and 14.0 GPa, respectively. The transition pressure decreases with increasing Mn content. The observed charge distribution of postspinel becomes an almost ideally ordered structure expressed by $^{VIII}[Mn^{2+}]^{VI}(Mn^{3+}_{0.5}Fe^{3+}_{0.5})_2O_4$, transformed from cubic Mn_2FeO_4 spinel.

(5) The magnetic refinements clarify the paramagnetic and ferrimagnetic structure of $MnFe_2O_4$ and Mn_2FeO_4 spinel as a function of pressure. The magnetic moment is ordered between A and B sites with the anti-parallel distribution along the *b* axis.

Supplementary Information The online version contains supplementary material available at https://doi.org/10.1007/s00269-022-01215-4.

Acknowledgements We would like to express our great thanks to Prof. Yukio Noda of Institute of Multidisciplinary Research for Advanced materials Tohoku University Japan and to Dr. Yoshihisa Ishikawa of Institute of Materials Structure Science KEK Japan for their fruitful discussion about magnetic structure. The present investigation was performed under the auspice of J-PARC Proposal No 2016B0018.

References

Akaogi M, Hamada Y, Suzuki T, Kobayashi M, Okada M (1999) High pressure transitions in the system Mg_2AlO_4 –$CaAl_2O_4$ a new hexagonal aluminous phase with implication for the lower mantle. Phys Earth Planet Inter 115:67–77

Akaogi M, Tajima T, Okano M, Kojitani H (2019) High-Pressure and High-temperature phase transitions in Fe_2TiO_4 and Mg_2TiO_4 with Implications for titanomagnetite inclusions in superdeep diamonds. Minerals 9(10):614

Andrault D, Casanova NB (2001) High-pressure phase transformations in the $MgFe_2O_4$ and Fe_2O_3-$MgSiO_3$ systems. Phys Chem Min 28:211–217

Åsbrink S, Waskowaka A, Olsen JS, Gerward L (1998) High-pressure phase of the cubic spinel $NiMn_2O_4$. Phys Rev B 57:4972–4974

Baron V, Gutzmer J, Rundlof H, Tellgren R (1998) The influence of iron substitution on the magnetic properties of hausmannite, Mn2+(Fe, Mn)3+2 O4. Am Min 83:786–793

Boucher B, Buhl R, Perrin M (1971) Magnetic structure of Mn_3O_4 by neutron diffraction. J Applied Physics 42:1615–1617

Chardon B, Vigneron F (1986) Mn_3O_4 commensurate and incommensurate magnetic structures. J Magn Magn Mater 58:128–134

Choi H, Shim JH, Min BI (2006) Electronic structures and magnetic properties of spinel $ZnMn_2O_4$ under high pressure. Phys Rev B 74:172103

Darul J, Lathe C, Piszora P (2013) Mn_3O_4 under high pressure and temperature: thermal stability, polymorphism, and elastic properties. J Phys Chem C 117:23487–23494

Dubrobinsky LS, Dubrovinskaia NA, McCammon R, Kh G, Ahuja R, Osorio-Guillen JM, Dmitriev V, Weber DP, Bihan TL, Johansson

B (2003) The structure of the metallic high pressure Fe_3O_4 polymorph experimental and theoretical study. J Phys: Condens Matter 16:7697

Dunitz JD, Orgel LE (1957) Electronic properties of transition-metal oxides I. Distortion from cubic symmetry. J Phys Chem Solids 3:20–29

Dunitz JD, Orgel LE (1960) Stereochemistry of ionic solids. Adv Inorg Chemis Radiochem 2:1–60

Errandonea D, Kumar RS, Manjon FJ, Ursaki VV, Rusa EV (2009) Post-spinel transformations and equation of state in $ZnGa_2O_4$: Determination at high-pressure by in situ x-ray diffraction. Phys Rev B 79:024103

Fei Y, Mao HK, Hemley RJ, Shu J, Shen G (1999) In situ structure determination of the high-pressure phase of Fe_3O_4. Am Miner 84:203–206

Gutzmer J, Beukes NJ, Kleyenstuberanda AS, Burger E (1995) Magnetic hausmannite from hydrothermally altered manganese ore in the paleoproterozoic kalahari manganese deposit, Transvaal super group, South Africa. Mineral Magazin 59:703–716

Haavik C, Sttoen S, Fjelvag H, Hanfland M, Häuserman D (2000) Equation of state of magnetite and its high-pressure modification: Thermodynamics of the Fe-O system at high pressure. Am Miner 85:514–523

Hasting JM, Corliss LM (1956) Neutron diffraction study of manganese ferrite. Phys Rev 104:328–331

Hattori T, Sano-Furukawa A, Arima H, Komatsu K, Yamada A, Inamura Y, Nakatani T, Seto Y, Nagai T, Utsumi W, Iitaka T, Kagi H, Katayama Y, Inoue T, Otomo T, Suzuya K, Kamiyama T, Arai M, Yagi T (2015) Design and Performance of High-Pressure PLANET Beamline at Pulsed Neutron Source at J-PARC. Nucl Instrum Methods Phys Res Sec A 780:55–67

Hattori T, Sano-Furukawa A, Machida S, Abe J, Funakoshi K, Arima H, Okazaki N (2019) Development of a technique for high-pressure neutron diffraction at 40 GPa with a Paris-Edinburgh press. High Press Res 39:417–425

Hirao N, Kawaguchi SI, Hirose K, Shimizu K, Ohtani E, Ohishi Y (2020) New developments in high-pressure X-ray diffraction beamline for diamond anvil cell at SPring-8. Matter Radiat Extremes 5:018403

Ishii T, Kojitani H, Tsukamoto S, Fujino K, Mori D, Inaguma Y, Tsujino N, Yoshino T, Yamazaki D, Higo Y, Funakoshi K, Akaogi M (2014) High-pressure phase transitions in $FeCr_2O_4$ and structure analysis of new postspinel $FeCr_2O_4$ and $Fe_2Cr_2O_5$ phases with meteoritic and petrological implications. Am Miner 99:1788–1797

Jackson JM, Strhahn W, Shen G, Zhao J, Hu MY, Errandonea D, Bass JD, Fei Y (2005) A synchrotron Mössbauer spectroscopy study of $(MgFe)SiO_3$ perovskite up to 120 GPa. Am Miner 90:199–205

Kirby SH, Stein S, Okai EA, Rubie DC (1996) Metastable mantle phase transformations and deep earthquakes in subducting oceanic lithosphere. Review of Geophysics 34:261–306

Kuriki A, Moritomo Y, Ohishi Y, Kato K, Nishibori E, Takata M, Sakata M, Hamada N, Todo S, Mori N, Shimomura O, Nakamura A (2002) High-pressure structure analysis of Fe_3O_4. J Phys Soc Japan 71:3092–3093

Kobayashi H, Isogai K, T., Hamada, N., Onodera, H. and Todo, S. (2006) Structure properties of magnetite under high pressure studied by Mössbauer spectroscopy. Phys Rev B 73(10):104110

Kyono A, Ahart M, Yamanaka T, Gramsch S, S., Mao, H.k. and Hemley, R.J. (2011a) High-pressure Raman spectroscopic studies of ulvöspinel Fe_2TiO_4. Am Mineral 96:1193–1198

Kyono A, Gramsch SA, Yamanaka T, Ikuta D, Ahart M, Mysen BO, Mao HK, Hemley RJ (2011b) The influence of the Jahn-Teller effect at Fe^{2+} on the structure of chromite at high pressure. Phys Chem Miner. https://doi.org/10.1007/s00269-011-0468-6

Larson AC, Von Dreele RB (2004) General Structure Analysis System (GSAS), Los Alamos National. Laboratory Report LAUR 86-748

Lavina B, Salviulo G, Giusta AD (1994) Cation distribution and structure modeling of spinel solid solutions. Phys Chem Miner 29:10–18

Levy D, Pastern L, Holster A, Visvovo G (2015) Thermal expansion and cation partitioning of $MnFe_2O_4$ (Jacobsite) from1.6 to1276K studied by using neutron powder diffraction. Solid State Chem 201:15–19

Lin JF, Speziale S, Mao Z, Marquardt H (2013) Effects of the electronic spin transitions of iron in lower-mantle minerals; implications to deep-mantle geophysics and geochemistry. Rev Geophys 51:244–275

Malavasi L, Tealdi C, Amboage M, Mozzatti MC, Flor G (2005) High pressure X-ray diffraction study of $MgMn_2O_4$ tetragonal spinel. Nuclear instrument and methods. Phys Res B 238:171–174

McMurdie HF, Sullvan BM, Maur FA (1950) High temperature X-ray study of the system Fe_3O_4–Mn_3O_4. J Res NIST 45:35–41

Muramatsu T, Gasparov LV, Berger H, Hemley RJ, Struzhkin VV (2016) Electrical resistance of single-crystal magnetite (Fe_3O_4) under quasi-hydrostatic pressures up to 100 GPa. J Appl Phys 119:135903

Murasik A, Roult G (1964) Structure magnetique du manganite de fer par diffraction neutronique. J De Phzs 25:522–525

Nakagiri N, Manghnani MH, Ming LC, Kimura S (1986) Crystal structure of magnetite under pressure. Phys Chem Minerals 13:238–244

Néel L (1948) Propriétés magnétiques des ferrites; ferrimagnétisme et antiferromagnétisme. Ann Phys (parris) 3:137

Ole´s, A., Kajzar, F., Kucab, M. and Sikora, W. (1976) Magnetic Structures. Panstwowe Wydawnictwo Naukowe, Determined by Neutron Diffraction

Paris E, Ross CR, Olijnyk H (1992) Mn_3O_4 at high pressure: a diamond-anvil cell study and a structural modeling. Eur J Mineral 4:87–93

Pasternak MP, Nasu S, Wada K, Endo S (1994) High-pressure phase of magnetite. Phys Rev B 50:6446

Prescher C, McCammon C, Dubrovinsky L (2012) MossA: a program for analyzing energy-domain Mössbauer spectra from conventional and synchrotron sources. J App Crystallogr 45:329–331

Reichmann HJ, Jacobsen SD (2004) High-pressure elasticity of a natural magneite crystal. Am Miner 89:1061–1066

Ricolleau A, Fei Y (2016) Equation of state of the high-pressure Fe_3O_4 phase and a new structural transition at 70 GPa. Am Miner 101:719–725

Rieck GD, Driessens FCM (1966) The structure of manganese-tron-oxygen spinels Acta. Crystallography 20:521–525

Rozenberg GK, Amiel Y, Xu WM, Pasternak MP, Jeanloz R, Hanfland M, Taylor RD (2007) Structure characterization of temperature-pressure-induced inverse normal spinel transformation in magnetite. Phys Rev B 75:020102

Sano-Furukawa A, Arima H, Yamada A, Tabata S, Kondo M, Nakamura A, Kagi H, Yagi T (2014) Six-axis multi-anvil press for high-pressure, high-temperature neutron diffraction experiments. Rev Sci Instrum 85:113905

Shannon RD, Prewitt CT (1969) Effective ionic radii in oxide and Fluorides. Acta Crystallogr B 25:935

Singh VK, Khatri NK, Lokanathan S (1981) Mössbauer study of ferrite systems $Co_xMn_{1-x}Fe_2O_4$ and $Ni_xMn_{1-x}Fe_2O_4$. Solid State Phys 16:273–280

Toby BH (2001) EXPGUI, a graphical user interface for GSAS. J Appl Crystallogr 34:210–213

Todo S, Takeshita N, Kanehara T, Mori T, Mori N (2001) Metallization of magnetite (Fe_3O_4) under high pressure. J Appl Phys 89:7347

Van Hook HJ, Keith ML (1958) The system Fe_3O_4-Mn_3O_4. Am Miner 43:69–83

Wang ZO, H, S.C., Lazor, P. and Saxena, S.K. (2002) High pressure Raman spectroscopic study of spinel $MgCr2O_4$. J Phys Chemis Solid 63:2057–2061

Wang Z, Downs RT, Pischedda V, Shetty R, Saxena SK, Zha CS, Zhao YS, Schiferl D (2003a) High-pressure x-ray diffraction and Raman spectroscopic studies of the tetragonal spinel $CoFe_2O_4$. Phys Rev B 66:024103

Wang Z, Schiferl D, Zhao Y, O'Neil H, St C (2003b) High pressure Raman spectroscopy of spinel-type ferrite $ZnFe_2O_4$. J Phys Chemis Solids 64:2517–2523

Waskowska A, Gerward L, Olsen JS, Steenstrup S, Talik E (2001) $CuMn_2O_4$: properties and the high-pressure induced Jahn-Teller phase transition. J Phys Condens Matter 13:2549–2562

Wickham DG (1969) The chemical composition of spinels in the system Fe_3O_4-Mn_3O_4. J Inorg Nucl Chem 31:313–320

Willerd M, Nakamura Y, Laughling DE, McHenry ME (1999) Magnetic properties of ordered and disordered spinel-phase ferrimagnets. J Am Ceram Soc 82:3342–3346

Wu Y, Wu X, Qin S (2012) Pressure-induced phase transition of Fe_2TiO_4: X-ray diffraction and Mössbauer spectroscopy. J Solid State Chem 185:72–75

Xu Y, Poe BT, Shankland J, Rubie DC (1998) Electrical conductivity of olivine, wadsleyite, and ringwoodite under upper mantle conditions. Science 280:1415–1418

Xu WM, Machavariani GYu, Rozenberg GKh, Paternak MP (2004) Mössbauer and resistivity studies of the magnetite and electronic properties of the high-pressure phase of Fe_3O_4. Phys Rev B 70:174106

Yafet Y, Kittel C (1952) Antiferromagnetic Arrangements in Ferrites. Phys Rev 87:290–294

Yamanaka T, Nakahira M (1973) Dependence of the cation distribution in manganese ferrite, $MnFe_2O_4$, on temperature and oxidation. Mineral J 73:202–220

Yamanaka T, Okita M (2001) Magnetic properties of the Fe_2SiO_4-Fe_3O_4 spinel solid solution. Phys Chem Min 28:102–109

Yamanaka T, Uchida A, Nakamoto Y (2008) Structural transition of postspinel phases $CaMn_2O_4$, $CaFe_2O_4$ and $CaTi_2O_4$ under high pressures up to 80 GPa. Am Miner 93:1874–1881

Yamanaka T, Kyono A, Nakamoto Y, Meng Y, Kharlamova S, Struzhkin VV, Mao HK (2013) High-pressure phase transitions of $Fe_{3-x}Ti_xO_4$ solid solution up to 60 GPa correlated with electronic spin transition. Am Miner 98:736–744

Yamanaka T, Rahman S, Nakamoto Y, Hattori T, Jang BG, Kim DY, Mao HK (2022) Enhancement of electrical conductivity to metallization of $Mn_{3-x}Fe_xO_4$ spinel and postspinel with elevating pressure. Phys Chem Solid. https://doi.org/10.1016/j.jpcs.2022.110721

Yasuoka H, Hirai H, Shinjo T, Kiyama M, Bando Y, Takada T (1967) NMR determination of metal ion distribution in manganese ferrite prepared from aqueous solution. J Phys Soc Jpn 22:174–180

Ye L, Zhai S, Wu X, Xu C, Yang K, Higo Y (2015) Compressibility of $MnFe_2O_4$ polymorphs. Phys Chem Miner 42:569–577